

10-2017

# Quantum fidelity approach to the ground-state properties of the one-dimensional axial next-nearest-neighbor Ising model in a transverse field

Oz de Alcantara Bonfim  
*University of Portland*, bonfim@up.edu

B. Boechat

J. Florencio

Follow this and additional works at: [https://pilotscholars.up.edu/phy\\_facpubs](https://pilotscholars.up.edu/phy_facpubs)



Part of the [Quantum Physics Commons](#)

---

## Citation: Pilot Scholars Version (Modified MLA Style)

Bonfim, Oz de Alcantara; Boechat, B.; and Florencio, J., "Quantum fidelity approach to the ground-state properties of the one-dimensional axial next-nearest-neighbor Ising model in a transverse field" (2017). *Physics Faculty Publications and Presentations*. 63. [https://pilotscholars.up.edu/phy\\_facpubs/63](https://pilotscholars.up.edu/phy_facpubs/63)

This Journal Article is brought to you for free and open access by the Physics at Pilot Scholars. It has been accepted for inclusion in Physics Faculty Publications and Presentations by an authorized administrator of Pilot Scholars. For more information, please contact [library@up.edu](mailto:library@up.edu).

# Quantum fidelity approach to the ground-state properties of the one-dimensional axial next-nearest-neighbor Ising model in a transverse field

O. F. de Alcantara Bonfim\*

*Department of Physics, University of Portland, Portland, Oregon 97203, USA*

B. Boechat† and J. Florencio‡

*Departamento de Física, Universidade Federal Fluminense, Avenida Litorânea s/n, Niterói, 24210-340, RJ, Brazil*

(Received 9 February 2017; revised manuscript received 7 September 2017; published 17 October 2017)

In this work we analyze the ground-state properties of the  $s = 1/2$  one-dimensional axial next-nearest-neighbor Ising model in a transverse field using the quantum fidelity approach. We numerically determined the fidelity susceptibility as a function of the transverse field  $B_x$  and the strength of the next-nearest-neighbor interaction  $J_2$ , for systems of up to 24 spins. We also examine the ground-state vector with respect to the spatial ordering of the spins. The ground-state phase diagram shows ferromagnetic, floating, and  $(2,2)$  phases, and we predict an infinite number of modulated phases in the thermodynamic limit ( $L \rightarrow \infty$ ). Paramagnetism only occurs for larger magnetic fields. The transition lines separating the modulated phases seem to be of second order, whereas the line between the floating and the  $(2,2)$  phases is possibly of first order.

DOI: [10.1103/PhysRevE.96.042140](https://doi.org/10.1103/PhysRevE.96.042140)

## I. INTRODUCTION

At very low temperatures, quantum fluctuations play an important role in the characterization of the ground-state properties of quantum systems [1]. These fluctuations are induced by varying the relative strength of competing interactions among the constituents of the system or by changing the strength of the applied fields. When large enough, quantum fluctuations dramatically change the nature of a given ground state. A quantum phase transition may occur, thereby creating a boundary between distinct ground states.

The one-dimensional axial next-nearest-neighbor Ising (1D ANNNI) model in a transverse field is one of the simplest models in which competing interactions lead to modulated magnetic orders, frustration, commensurate-incommensurate transitions, etc. These features are known to appear in the ground state of the model in the one-dimensional case.

Frustration in the 1D ANNNI model arises from the competition between nearest-neighbor interactions which favor ferromagnetic alignment of neighboring spins, while an interaction with opposite sign between the next-nearest-neighbors fosters antiferromagnetism. At  $T = 0$ , the presence of a transverse magnetic field gives rise to quantum fluctuations that play an analogous role to that of temperature in thermal magnetic systems that are responsible for triggering phase transitions.

In one dimension, the ANNNI model in a transverse field is actually an extension of the transverse Ising model. The latter consists of Ising spins with nearest-neighbor interactions in the presence of a magnetic field in the transverse direction. The transverse Ising model was initially used to explain the order-disorder transitions observed in KDP ferroelectrics [2]. An experimental realization of that model in real magnetic systems was observed in  $\text{LiHoF}_4$  in an external field [3]. An exact solution to the model in one dimension was subsequently found

by Pfeuty by mapping the set of the original spin operators onto a new set of noninteracting spinless Fermi operators [4]. Recently, a degenerate Bose gas of rubidium confined in a tilted optical lattice was used to simulate a chain of interacting Ising spins in the presence of both transverse and longitudinal fields [5]. It has also been proven that the ground-state properties of the  $d$ -dimensional Ising model with a transverse field are equivalent to those of the  $(d + 1)$ -dimensional Ising model without a magnetic field at finite temperatures [6–8].

In the case of the 1D ANNNI model in a transverse field at  $T = 0$  and the 2D ANNNI model (without transverse field) at finite  $T$ , such equivalence may only exist in the limit of very strong transverse field and in the weak-coupling limit of the NN and NNN interactions of the 1D model [9–11]. There is no guarantee that the ground-state phase diagrams of those models bear any resemblances to each other. Therefore we shall not compare the phase diagrams of these two models in this work.

The transverse 1D ANNNI model has been the subject of great interest [12,13], in part due to the number of quantum phases with unusual and intriguing features that it displays. Several analytical and numerical methods have been employed to establish its phase diagram. Among these studies, there are analysis using quantum Monte Carlo [14], exact diagonalization of small lattice systems [15,16], the interface approach [17], scaling behavior of the energy gap [18], bosonization and renormalization group methods [19], density matrix renormalization group [20,21], perturbation theory [22], and matrix product states [23].

The phase diagrams from those works do not necessarily agree with each other. In the following we discuss the common features as well as some of the differences between them. In most of the studies, there is ferromagnetism for  $J_2 < 0.5$  and the  $(2,2)$  antiphase for  $J_2 > 0.5$ . The transition lines usually end at the multicritical point  $(J_2, B_x) = (0.5, 0.0)$ . The phase diagram of Dutta and Sen shows antiferromagnetism instead of the  $(2,2)$  antiphase for  $J_2 > 0.5$  [19]. This is a rather surprising result, not to show the antiphase, since even in the classical case,  $B_x = 0$ , that antiphase is energetically favorable. Some

\*bonfim@up.edu

†bmbp@if.uff.br

‡jfj@if.uff.br

authors obtain diagrams with 5 phases, namely, ferromagnetic, paramagnetic, modulated paramagnetic, floating, and antiphase. Such are the diagrams of Arizmendi *et al.* [14], Sen *et al.* [15], and Beccaria *et al.* [20,21]. On the other hand, Rieger and Uimin [16], Chandra and Dasgupta [22], and Nagy [23] present diagrams with 4 phases, ferromagnetic, paramagnetic, floating, and antiphase. In Refs. [16,23] the boundary lines meet at the multicritical point, whereas in Ref. [22] the paramagnetic phase is restricted to sufficiently high  $B_x$ ; thus its boundary lines do not reach the multicritical point. In the studies by Sen [17] and Guimarães *et al.* [18], one finds diagrams with 3 phases only, ferromagnetic, paramagnetic, and antiphase, where their transition lines end at the multicritical point. The phase diagram of Dutta and Sen [19] displays ferromagnetism, a spin-flop phase, a floating phase, and an antiferromagnetic phase. In that work, the floating phase lies between the antiferromagnetic and the spin-flop phases. Such spin-flop and antiferromagnetic phases do not appear in any of the other phase diagrams in the literature. In addition, their transition lines do not end at the multicritical point. As one can see, there is no consensus on the ground-state phase diagram of the model. The number, nature, or location of the phases usually vary from one work to another. In any case, all the studies in the literature report on a finite number of phases. As we shall see below, our phase diagram agrees with some of the works in the literature with regard to the existence of ferromagnetic, floating, and the antiphase. However, our numerical results suggest that there are an infinite number of modulated phases between the ferromagnetic and the floating phase. Such scenario is similar to the one found in the the work of Fisher and Selke [24] on the low-temperature phase diagram of an Ising model with competing interactions. In that study the phase diagram shows an infinite number of commensurate phases.

While the identification of the usual thermal phase transitions relies mostly on the behavior of an order parameter or on an appropriate correlation function, quantum phase transitions can also be characterized solely by the properties of the ground-state eigenvectors of the system on each side of the boundary between two competing quantum mechanical states. We use fidelity susceptibility to determine the phase boundary lines, as well as a direct inspection of the eigenvectors to understand the nature of the phases. In our work, paramagnetism only occurs at high fields  $B_x$ ; hence it does not appear in our phase diagram, which covers the low-field region only. In addition, our numerical analysis points to the existence of a region of finite width for the floating phase.

## II. THE MODEL

The one-dimensional ANNNI model in the presence of a transverse magnetic field is defined as

$$\mathcal{H} = -J_1 \sum_i \sigma_i^z \sigma_{i+1}^z + J_2 \sum_i \sigma_i^z \sigma_{i+2}^z - B_x \sum_i \sigma_i^x. \quad (1)$$

The system consists of  $L$  spins, with  $s = 1/2$ , where  $\sigma_i^\alpha$  ( $\alpha = x, y, z$ ) is the  $\alpha$  component of a Pauli operator located at site  $i$  in a chain where periodic boundary conditions are imposed. We considered ferromagnetic nearest-neighbor Ising coupling  $J_1 > 0$  and antiferromagnetic next-nearest-neighbor

interaction  $J_2 > 0$ .  $B_x$  is the strength of a transverse applied magnetic field along the  $x$  direction. We set  $J_1 = 1$  as the unit of energy.

At  $T = 0$  and in the absence of an external magnetic field ( $B_x = 0$ ), the model is trivially solvable and presents several ordered phases. For  $J_2 < 0.5$ , the ground-state ordering is ferromagnetic, and for  $J_2 > 0.5$ , the ordering changes to a periodic configuration with two up-spins followed by two down-spins which is termed the  $\langle 2,2 \rangle$  phase, or antiphase. In this work we have used the notation  $\langle p,q \rangle$  to represent a periodic phase, with  $p$  up-spins followed by  $q$  down-spins. At  $J_2 = 0.5$ , the model has a multiphase point where the ground state is infinitely degenerate and a large number of  $\langle p,q \rangle$  phases are present, as well as other spin configurations. The number of phases increases exponentially with the size of the system [25,26]. On the other hand, for a nonzero external magnetic field and  $J_2 = 0$ , the model reduces to the Ising model in a transverse field, which was solved exactly by Pfeuty [4]. The transverse magnetic field induces quantum fluctuations that eventually drive the system through a quantum phase transition. Its ground state undergoes a second-order quantum phase transition at  $B_x = 1$ , separating ferromagnetic from paramagnetic phases. In the 1D transverse ANNNI model, next-nearest-neighbor interactions introduce frustration to the magnetic order. A much richer variety of phases becomes possible when one varies the strength of the interactions among the spins or their couplings to the magnetic field.

Given that so far there has not been a definite answer to the problem of the ground-state properties of the transverse ANNNI model, where different approaches yield distinct phase diagrams, we use the quantum fidelity method together with direct inspection of the ground-state eigenvector to shed some light on the problem. We believe our approach is suitable because both the fidelity susceptibility and ground-state eigenvector provide detailed direct information about the boundary and nature of the ground-state phases. We investigate how the phase diagram evolves as we consider larger and larger lattices. Our results are consistent with some known results, such as the classical multicritical point, the Pfeuty quantum transition point, and the exact Peschel-Emery line which runs between those two points in the phase diagram [27]. From our results for finite-sized systems we can infer which phases will be present in the thermodynamic limit.

## III. THE FIDELITY METHOD

Suppose the Hamiltonian of the system depends on a parameter  $\lambda$ , which drives the system through a quantum phase transition at a critical value  $\lambda = \lambda_c$ . Quantum fidelity is defined as the absolute value of the overlap between neighboring ground states of the system [28,29],

$$F(\lambda, \delta) = |\langle \psi(\lambda - \delta) | \psi(\lambda + \delta) \rangle|. \quad (2)$$

Here  $|\psi\rangle$  is the quantum nondegenerate ground-state eigenvector that is evaluated at some value of  $\lambda$ , shifted by an arbitrary small quantity  $\delta$  around it. In addition to the dependence on  $\lambda$  and  $\delta$ , the quantum fidelity is also a function of the size of the system. The basic idea behind the fidelity approach is that the overlap of the ground state for values of the parameter

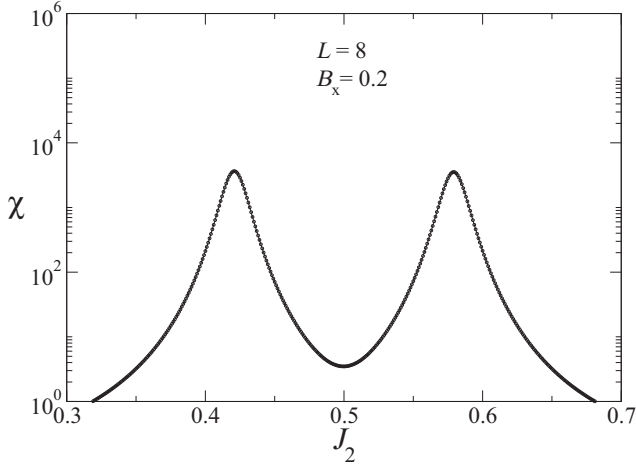


FIG. 1. Fidelity susceptibility as a function of the next-nearest-neighbor coupling  $J_2$  for the transverse ANNNI model with  $B_x = 0.2$ , for the case of a chain with  $L = 8$  spins. Here, and also in the next figures,  $J_1 = 1$  is set as the energy unit. The locations of the peaks give the transition points.

$\lambda$  between the two sides of a quantum transition exhibits a considerable drop due to the distinct nature of the ground states on each side of the phase boundary. Quantum fidelity has been used in quantum information theory [30] as well as in condensed matter physics, in particular in the study of topological phases [31,32].

For a fixed value  $L$  and in the limit of very small  $\delta$ , the quantum fidelity may be written as a Taylor expansion,

$$F(\lambda, \delta) = 1 - \chi(\lambda)\delta^2 + O(\delta^4), \quad (3)$$

where the ground-state eigenvector is normalized to unity. The quantity  $\chi(\lambda)$  is called the fidelity susceptibility and will reach a maximum at the boundary between adjacent quantum phases. We used the fidelity susceptibility to find the phase boundary lines on the  $(J_2, B_x)$  plane and compare them with the results obtained by other methods.

To determine the ground-state energy and eigenvector as a function of  $\lambda$ , we employed both Lanczos and the conjugate-gradient methods. The latter is known to be a fast and reliable computational algorithm. It has been used in statistical physics, especially in the context of Hamiltonian models and of transfer-matrix techniques [33,34]. Both methods give the same ground-state eigenvalues and eigenstates within a given precision. Depending on the size of the system, the ground-state energy is calculated with precision between  $10^{-10}$  and  $10^{-12}$ . We have used  $\delta = 0.001$  in all calculations involving the fidelity susceptibility. For the location of each point at the critical boundary, we calculated the maximum value of the fidelity susceptibility as defined by Eq. (3).

In order to identify the nature of the quantum phase, we examined how the ground-state eigenvectors are written in terms of a complete set of appropriate basis vectors. To find the eigenstates and corresponding eigenvalues of the system we needed to choose a complete set of orthogonal basis vectors and write the Hamiltonian in matrix form using this basis set. The eigenvalues and eigenstates are found by exact numerical diagonalization. A convenient basis consists of the tensor

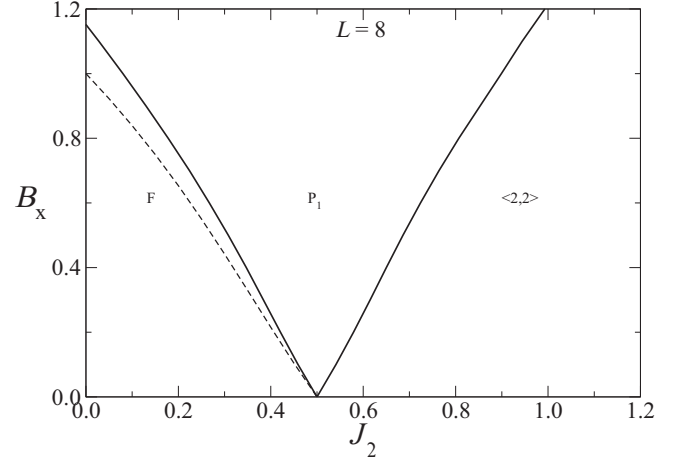


FIG. 2. Phase diagram in the  $(J_2, B_x)$  plane for a system of size  $L = 8$ . The system displays three phase regions, ferromagnetic  $F$ ,  $P_1$ , and  $\langle 2,2 \rangle$ . No additional phases are present here. The dashed boundary is the exact Peschel-Emery line.

product of  $L$  eigenstates of the  $z$  component of the local spin operator acting on each site. We denote the eigenstates by  $|s\rangle_i$ , where  $s = 1$  is the eigenstate label of the operator  $\sigma_i^z$  for an up-spin and  $s = 0$  for the a down-spin at site  $i$ . A generic basis eigenstate for the full system with  $L$  spins can be written as  $|n\rangle = \prod_i^L |s\rangle_i$ , where  $n$  labels the basis state and has the values  $n = 0, 1, \dots, N - 1$ , and where  $N = 2^L$  represents the dimension of the Hilbert space. The basis index  $n$ , if written in binary notation, can also be used to specify the configuration of the spins forming that basis. That is, when  $n$  is written in binary notation, the position and value of a bit will indicate whether the spin at that position (site) is up (1) or down (0). For instance, for a chain of 12 spins the state  $|1755\rangle$  in binary notation is written as  $|011011011011\rangle$ , which represents a periodic configuration with one down-spin (0) followed by two up-spins (11). In this notation, an arbitrary eigenstate of the Hamiltonian may be cast as

$$|\phi_\alpha\rangle = \sum_{n=0}^{N-1} a_\alpha(n)|n\rangle, \quad (4)$$

where  $\alpha = 0, \dots, N - 1$  labels the quantum states, with  $\alpha = 0$  assigned to the ground state. Since the matrix Hamiltonian is real and symmetric, the coefficients  $a_\alpha(n)$  are real. As a result, the quantum state  $|\phi_\alpha\rangle$  can be visualized in a single graph by plotting  $a_\alpha(n)$  as a function of the quantum-state index  $n$ . The graph will completely identify the spatial distribution of spins in the quantum state [35–37].

#### IV. RESULTS

In the following we present our results for system sizes  $L = 8, 12, 16, 20$ , and  $24$ . We chose those sizes in order to avoid the effects of frustration and preserve the symmetry of the  $(2,2)$  antiphase, which has periodicity of 4 lattice spacings. Still we are able to draw reliable conclusions as well as predictions about the quantum model in the thermodynamic limit.

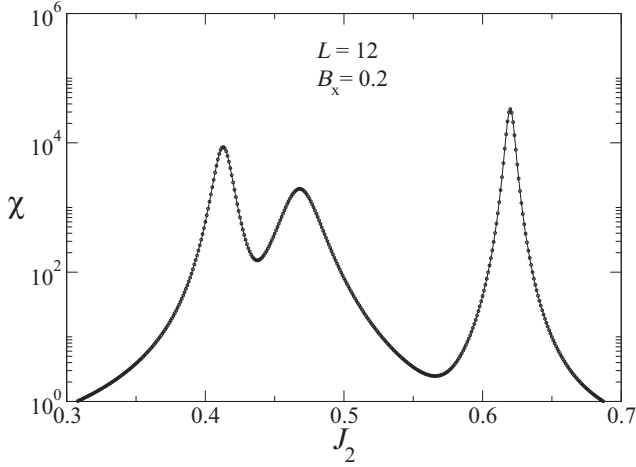


FIG. 3. Fidelity susceptibility as a function of next-nearest-neighbor coupling  $J_2$ , with  $B_x = 0.2$ , for the case  $L = 12$  spins. The locations of the peaks give the transition points.

Let us consider first the case  $L = 8$ . Figure 1 shows the fidelity susceptibility plotted against the next-nearest-neighbor interaction  $J_2$  for a fixed transverse field  $B_x = 0.2$ . The two peaks in the graph give the locations of the critical points where quantum phase transitions occur. By calculating the susceptibility for several values of  $B_x$  and  $J_2$ , we obtain the phase diagram shown in Fig. 2. There, we readily identify three distinct phases for low magnetic fields. The region farthest to the left ( $F$ ) is ferromagnetic, while the middle ( $P_1$ ) has a modulated phase, and the region farthest to the right has the antiphase ( $\langle 2,2 \rangle$ ). The transition line bordering the ferromagnetic phase is close to the exact Peschel-Emery line [27]. As we shall see, for larger system sizes we obtain results which are closer to that line. Notice that all the phase boundary lines meet at  $(J_2, B_x) = (0.5, 0.0)$ , the known multicritical point. Finally, for large enough magnetic fields, the modulated phase becomes paramagnetic. Such a feature does not appear in the phase diagram shown, which covers relatively low

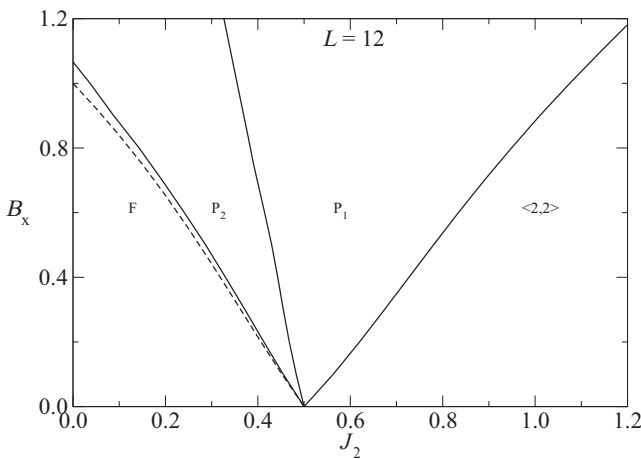


FIG. 4. Phase diagram in the  $(J_2, B_x)$  plane. The system displays four phase regions, ferromagnetic  $F$ ,  $P_1$  and  $P_2$ , and  $\langle 2,2 \rangle$ . Again, the dashed boundary is the Peschel-Emery line.

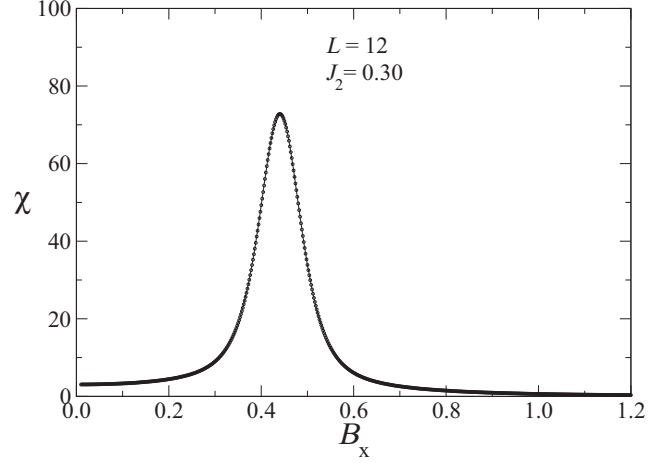


FIG. 5. Fidelity susceptibility as a function of the transverse field  $B_x$  for the transverse ANNNI model with  $J_2 = 0.30$ , for the case of a chain with  $L = 12$  spins. The location of the peak gives the transition point.

magnetic fields, where lies the interesting physics. That is also true for all the following phase diagrams below, which are valid at the low-field region, where we are concerned with the onset and further evolution of modulated phases as the system size increases.

Consider now  $L = 12$ . Figure 3 shows the fidelity susceptibility versus  $J_2$ , for  $B_x = 0.2$ . The three peaks on the graph give the locations where the phase transitions occur. Proceeding in a similar way for various values of  $B_x$  we determine the phase diagram, which is shown in Fig. 4. Alternately, by keeping  $J_2$  fixed and sweeping with  $B_x$  we obtain the same phase diagram. As an example of this we present Figs. 5, 6, and 7, which show the susceptibilities along  $B_x$ . The peaks are at the same locations as those obtained earlier with  $J_2$  sweeps. As can be seen, there appears an additional phase boundary line, as compared to the case  $L = 8$ . There is a modulated phase in the region  $P_2$ , and a floating

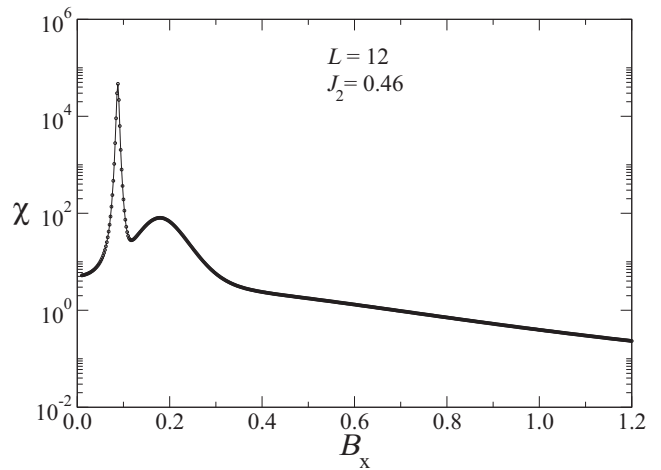


FIG. 6. Fidelity susceptibility versus the transverse field  $B_x$ , for  $J_2 = 0.46$ , in the case  $L = 12$ . The locations of the peaks give the transition points.

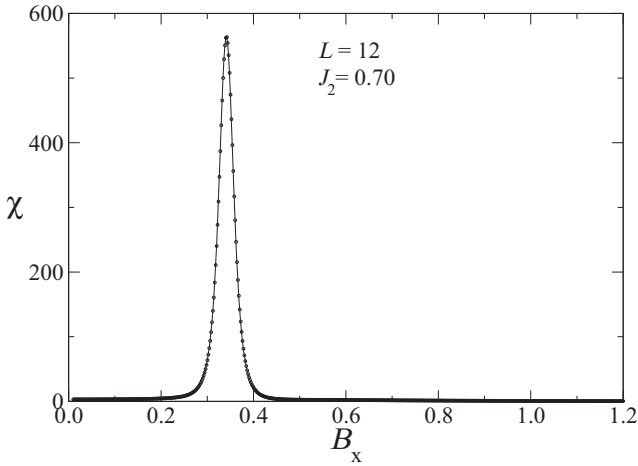


FIG. 7. Fidelity susceptibility as a function of the transverse field  $B_x$ , with  $J_2 = 0.70$ , for the case  $L = 12$ . The location of the peak gives the transition point.

phase  $P_1$ . These phases are separated by the boundary line that meets at the multicritical point. For very large fields  $B_x$  we expect the system to be paramagnetic. The ferromagnetic and antiphase regions remain basically the same, apart from a slight shift in their borders, due to finite-size effects. The boundary line between the ferromagnetic and its neighboring modulated phase is now closer to the Peschel-Emery line than that of the case  $L = 8$ .

The spin configurations in each of the phases can be inferred from a plot of the amplitudes  $a_0(n)$  of the ground-state eigenvector versus the basis index  $n$  for a point deep within a given phase. For instance, consider the point in the phase diagram  $(J_2, B_x) = (0.345, 0.200)$ , which is in the  $F$  phase. Figure 8 shows  $a_0(n)$  vs  $n$  for that point. The two largest contributions to the ground state correspond to the ferromagnetic spin configurations,  $n = 0$  and  $n = 4095$ , which have binary representations  $|000000000000\rangle$  and  $|111111111111\rangle$ , respectively. The other basis states with smaller amplitudes are induced

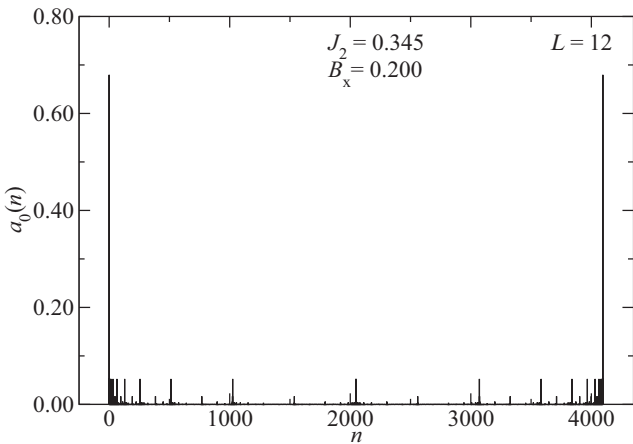


FIG. 8. Ground-state amplitude versus the basis-state index  $n$  for  $(J_2, B_x) = (0.345, 0.200)$ , within the phase  $F$  for  $L = 12$ . The two largest amplitudes correspond to the ferromagnetic phase. The smaller amplitudes are induced by the transverse magnetic field.

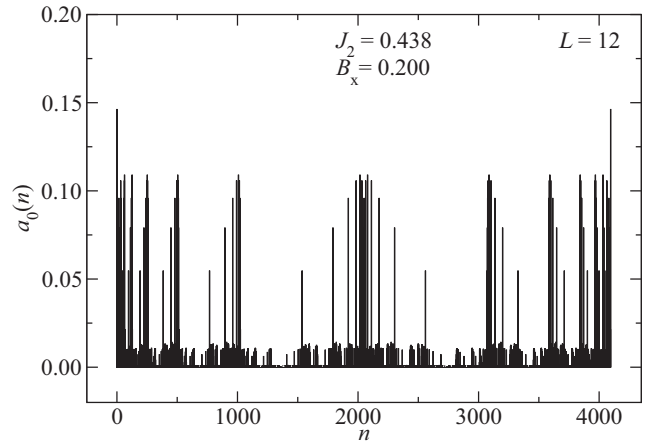


FIG. 9. Ground-state amplitude for each basis-state index  $n$ , with  $(J_2, B_x) = (0.438, 0.200)$ , located inside the phase region  $P_2$ , for  $L = 12$ . The two largest amplitudes correspond to a ferromagnetic phase. The next largest amplitudes are from states with a single kink separating ferromagnetic domains.

by the transverse magnetic field. Those amplitudes increase with  $B_x$ . Consider now  $(J_2, B_x) = (0.438, 0.200)$ , which lies in the region  $P_2$  of Fig. 4. The amplitudes of the ground-state basis vectors are depicted in Fig. 9. The largest contributions come from ferromagnetic orderings, while the second largest amplitudes are from the basis state  $|000000111111\rangle$  and its cyclic permutations of the spins. The third largest amplitudes are very close to the second. They come from the states  $|000000011111\rangle$ ,  $|111111100000\rangle$ , and all the others were obtained by their cyclic relatives. The boundary line separating the  $F$  phase from the neighboring modulated phase starts out at the multiphase point  $(J_2, B_x) = (0.5, 0.0)$  and ends close to the Pfeuty transition point  $(J_2, B_x) = (0.0, 1.0)$ .

We find that as the transverse field becomes sufficiently large the system enters a paramagnetic phase, where the spins tend to point in the same direction as the field. This is a general feature of the model. No matter which phase the system is in when  $B_x$  is small, eventually it will become paramagnetic as the field increases. We do not find any evidence of a sharp transition to paramagnetism. It seems that paramagnetism is achieved through a crossover mechanism, so that no transition line is observed. Figure 10 shows the ground-state eigenvector amplitudes for 3 cases:  $B_x = 0.200$ ,  $2.000$ , and  $20.00$ . The figures were obtained for  $L = 12$  and  $J_2 = 0.565$ , but similar behavior is expected for any other set of parameters  $L$  and  $J_2$ . The top figure ( $B_x = 0.2$ ) shows the 6 largest amplitudes that correspond to those basis vectors containing periodic sequences of 3 up- followed by 3 down-spins. The next largest amplitudes stem from spin arrangements not periodic. As the field becomes sufficiently large, the amplitudes for the ordered phase disappear, while all the other amplitudes becomes larger, as can be seen in the middle panel of Fig. 10. There, most of the spins are equally likely to align themselves with the transverse field. Finally, for very large fields (e.g.,  $B_x = 20.00$ ), nearly all the spins align themselves with the field, resulting in a more evenly distributed amplitude of the basis vectors. Clearly the system is in an induced paramagnetic phase. As we shall see later, when we consider larger lattices,

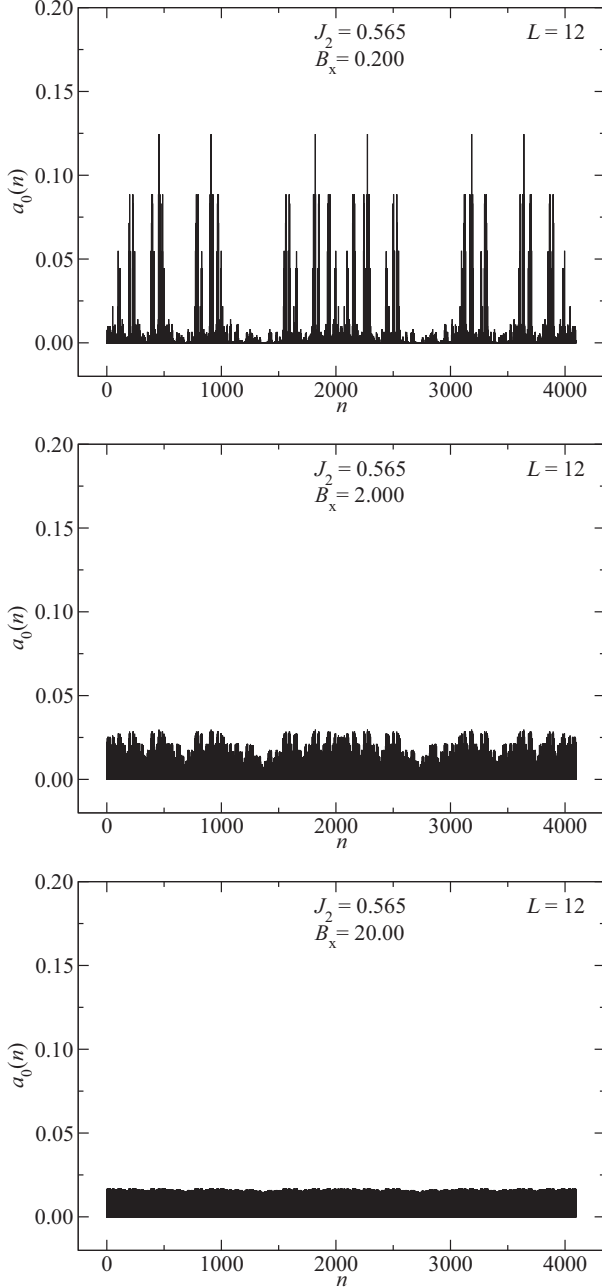


FIG. 10. Amplitude of the ground state against the basis-state index  $n$  for the case  $L = 12$ ,  $J_2 = 0.565$ , and different values of  $B_x$ . Top:  $B_x = 0.200$ , which lies in the phase region  $P_1$  in Fig. 4. The six highest amplitudes correspond to a  $\langle 3,3 \rangle$  phase, while the next-highest amplitudes belong to states without sequential order for the spins. Middle:  $B_x = 2.000$ ; here there are no noticeable prominent amplitudes, since the system is already in an induced paramagnetic state, where the spins are mostly aligned to the transverse field. Bottom: Case  $B_x = 20.00$ ; now nearly all the spins are aligned with the transverse field.

nonperiodic configurations will dominate the low- $B_x$  phase. That amounts to the so-called floating phase. In that phase there is not any periodic spin order commensurate with the underlying lattice.

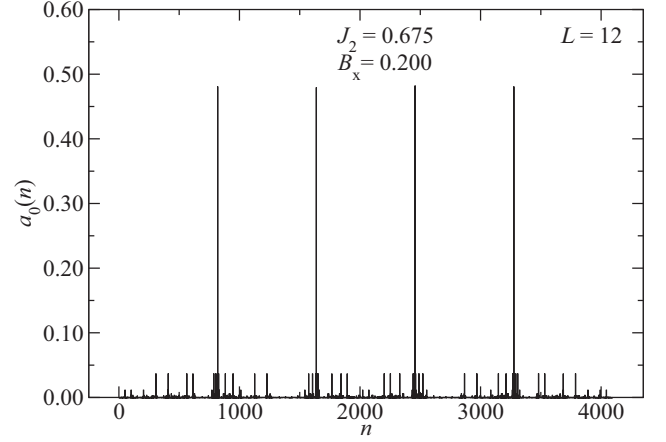


FIG. 11. Amplitude of the ground state for each of the basis-state indexes  $n$  when  $(J_2, B_x) = (0.675, 0.200)$ , within the phase  $\langle 2,2 \rangle$  for  $L = 12$ . The four largest amplitudes correspond to the  $\langle 2,2 \rangle$  phase. The transverse magnetic field is responsible for the appearance of the smaller amplitudes.

Finally, the ground state of the rightmost phase in Fig. 4 is dominated by four amplitudes corresponding to the  $\langle 2,2 \rangle$  phase. The dependence of the amplitudes on the state index for  $(J_2, B_x) = (0.675, 0.200)$  in that phase is depicted in Fig. 11. Again, small amplitudes are due to the transverse magnetic field and, as in the other cases, and they get larger as  $B_x$  increases.

Both the  $F$  phase and the  $\langle 2,2 \rangle$  phase are present in all the cases we considered ( $B_x \leq 1.2$ ), for all lattice sizes  $L$ . They are expected to be present in the thermodynamic limit. This is in agreement with the results found by other methods [14,18,20–23]. However, as we consider larger lattices, other modulated phases appear in between the ferromagnetic and the floating phase. It should be noted that all the transition lines start out at the multiphase point and then spread outwards as  $B_x$  increases. For sufficiently large  $B_x$  the phase is expected to be paramagnetic.

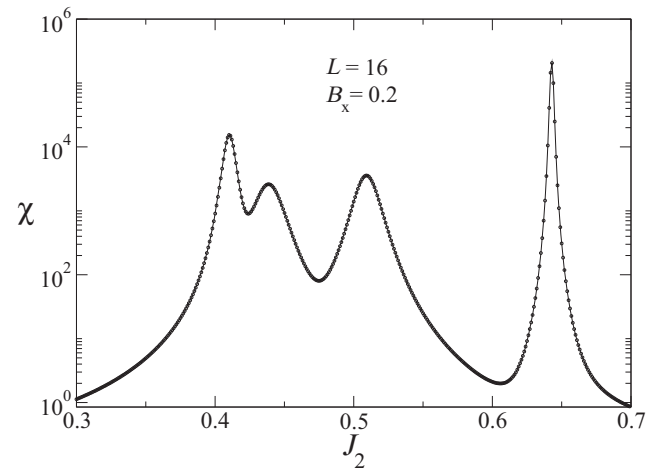


FIG. 12. Fidelity susceptibility as a function of the next-nearest-neighbor coupling for the case  $L = 16$ . The four peaks shown are centered at the transition points. Here  $B_x = 0.2$ .

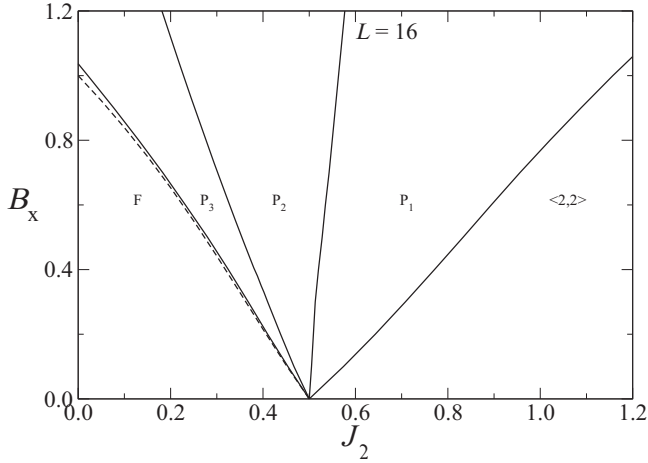


FIG. 13. Phase diagram in the  $(J_2, B_x)$  plane for the case  $L = 16$ . The figure shows the phase regions  $F$ ,  $P_1$ ,  $P_2$ ,  $P_3$ , and  $\langle 2,2 \rangle$ . The dashed boundary is the exact Peschel-Emery line.

Let us consider now the model with size  $L = 16$ . Figure 12 shows the fidelity susceptibility as a function of  $J_2$ , for  $B_x = 0.2$ . The susceptibility exhibits four peaks, thus indicating five distinct phases. Again, by numerically varying  $B_x$  and  $J_2$ , we obtained the phase diagram for the system, depicted in Fig. 13. At the two far sides of the diagram we obtained the  $F$  and  $\langle 2,2 \rangle$  phases, as in the previous case. The positions of the boundaries of the  $F$  and  $\langle 2,2 \rangle$  phases with their neighboring phases are weakly dependent on the system size, especially the boundary of the  $F$  phase. The slope of the boundary line of the  $\langle 2,2 \rangle$  phase for  $L = 16$  diminishes a little as compared with the previous case  $L = 12$ . We find an additional modulated phase, which is dominated by states with the ordered pattern  $\langle 4,4 \rangle$ . There appears to be other contributions to the ground state of much smaller weights which are not ordered, but which will increase with the applied field  $B_x$ . Again, all the transition lines start at the multicritical point.

For  $L = 20$  and  $B_x = 0.2$  the fidelity susceptibility shows 5 peaks, as seen in Fig. 14. The plot indicates the existence of five phase transitions for this lattice size. The phase diagram  $J_2 - B_x$  is shown in Fig. 15. We observe that another modulated phase has appeared. Now, in addition to the ferromagnetic, floating, and  $\langle 2,2 \rangle$  antiphase, the system has three modulated phases. The floating phase  $P_1$  for this lattice size is dominated by the orderings  $\langle 3,2 \rangle$  and  $\langle 2,3 \rangle$ . Again, the modulated phases eventually become paramagnetic for large enough transverse fields.

For larger system sizes, we observe a pattern that allows us to make inferences about the phases of the system in the thermodynamic limit. Due to computer limitations, the largest system studied is  $L = 24$ . Figure 16 shows the fidelity susceptibility as a function of  $J_2$ , for  $B_x = 0.2$ . There are 6 peaks, indicating an equal number of phase transitions. The phase diagram is shown in Fig. 17. We now identify 4 modulated phases in the figure,  $P_2$ ,  $P_3$ ,  $P_4$ , and  $P_5$ , in addition to the floating  $P_1$ , ferromagnetic  $F$ , and  $\langle 2,2 \rangle$  phases. The paramagnetic phase only occurs for high  $B_x$ , where the phases lose their characteristics as the spins tend to align with the transverse field. The modulated phases are

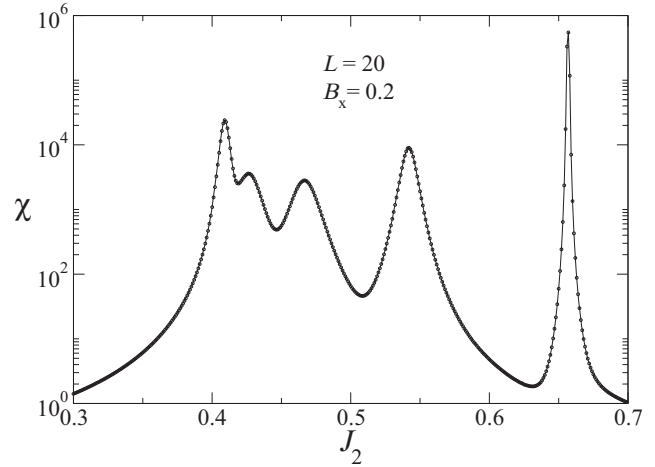


FIG. 14. Fidelity susceptibility as a function of next-nearest-neighbor coupling  $J_2$  for  $B_x = 0.2$  in the case  $L = 20$ . The five peaks are centered at the transition points.

characterized by several periodicities, among them  $\langle 4,4 \rangle$  for  $P_3$ , and  $\langle 3,3 \rangle$  for  $P_2$ . The floating phase  $P_1$  is now dominated by configurations which do not exhibit any periodicity within the system size. No particular ordering seems to take place as  $L$  increases; hence no commensurate order emerges in the floating phase.

As the system size increases, more modulated phases appear. For sufficiently large transverse magnetic fields one expects the system to become paramagnetic. The origin of the modulated phases follows from the degeneracy of the ground state at  $J_2 = 0.5$  and  $B_x = 0.0$ . There, the ground state is highly degenerate, with the number of configurations exponentially increasing with the size of the system, as mentioned before. The transverse magnetic field lifts the degeneracies, thus separating the phases. At finite sizes, some of the phases become visible. As one considers larger systems,

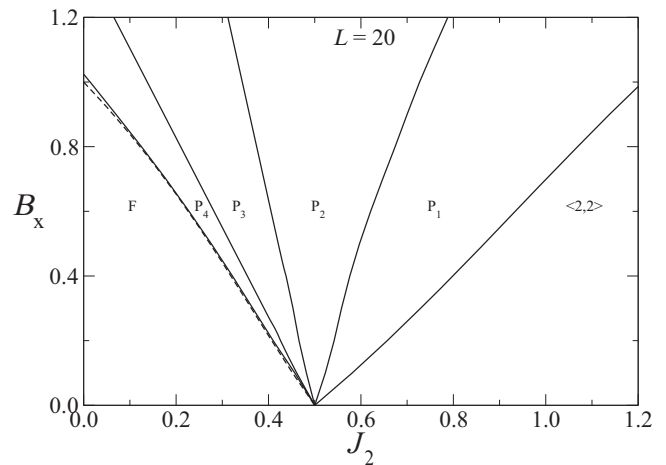


FIG. 15. Phase diagram in the  $(J_2, B_x)$  plane when the system size is  $L = 20$ . In addition to the phases  $F$  and  $\langle 2,2 \rangle$ , at the left and right of the diagram, respectively, there are four phases in between them, namely  $P_1$ ,  $P_2$ ,  $P_3$ , and  $P_4$ . The dashed boundary is the exact Peschel-Emery line.



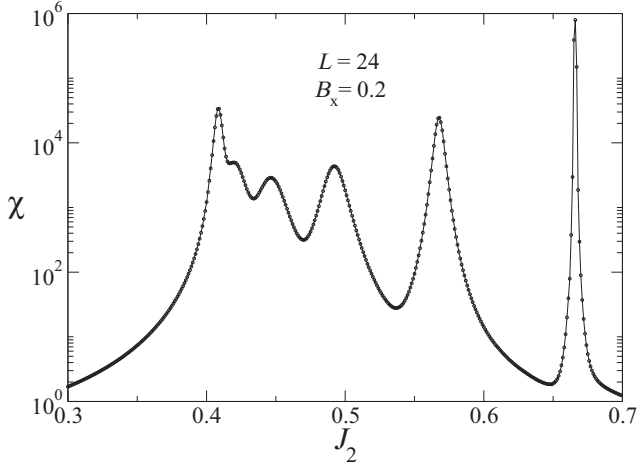


FIG. 16. Fidelity susceptibility as a function of next-nearest-neighbor coupling  $J_2$  for the case  $L = 20$ . The six peaks are centered at the transition points. Here  $B_x = 0.2$ .

more of those phases appear. The ferromagnetic as well as the  $\langle 2,2 \rangle$  phases should be obviously present for any system size in the cases  $J_2 < 0.5$  and  $J_2 > 0.5$ , respectively, since they are energetically favorable in those situations. Our numerical analysis was done with a maximum of 24 spins due to computer limitations. Yet, we can expect that as the number of spins increases there will appear more and more distinct modulated phases. We predict that at the thermodynamic limit there will be an infinite number of modulated phases.

At criticality the fidelity susceptibility shows power-law behavior with the lattice size, indicating that the transition is of second order; otherwise it is of first order [38]. For instance, for the transition line closest to the ferromagnetic phase we observe a power-law behavior, which is shown in Fig. 18. The solid line is the numerical fit  $\chi = 59.2L^2$ . It seems that all the transition lines between modulated phases are of second

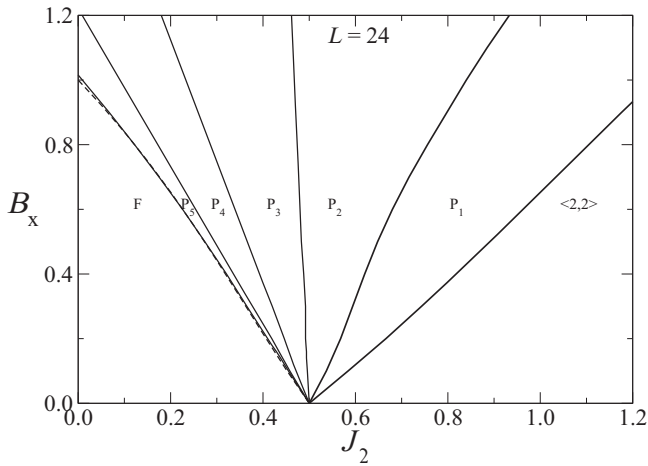


FIG. 17. Phase diagram in the  $(J_2, B_x)$  plane when the system size is  $L = 24$ . In addition to the phases  $F$  and  $\langle 2,2 \rangle$ , at the left and right of the diagram, there are five phases in between them, namely  $P_1, P_2, P_3, P_4$ , and  $P_5$ . The dashed boundary is the exact Peschel-Emery line, which lies very close to transition line between  $F$  and  $P_5$ .

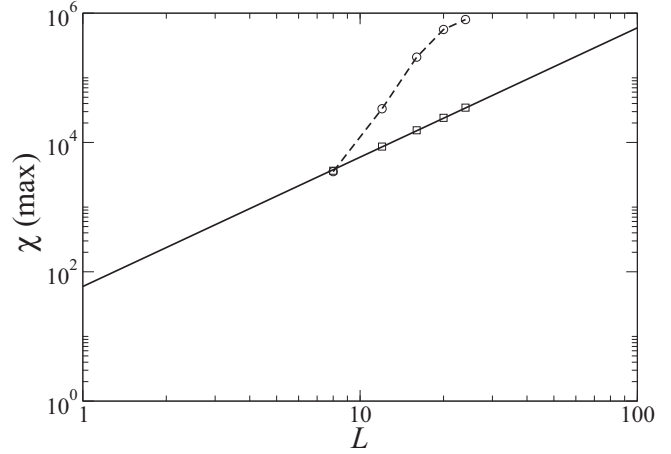


FIG. 18. Fidelity susceptibility at criticality as a function of the lattice size  $L$  for two different transition lines. Squares are for the transition line bordering the ferromagnetic phase (Peschel-Emery line) while circles are for the antiphase.

order. In particular, the transition between the modulated phase  $P_2$  and the floating phase ( $P_1$ ) seems to be of second order, contrary to the claims that it is of BKT type. Finally, the transition line separating the floating and  $\langle 2,2 \rangle$  antiphase is of first order, since the behavior of the susceptibility deviates from power law, as can be seen in Fig. 18.

The scaling behavior of the fidelity susceptibility in the vicinity of a quantum critical point has been found to be [39,40]

$$\chi(\lambda_c) \sim L^{2/\nu}, \quad (5)$$

where  $\nu$  is the critical exponent describing the divergence of the correlation function. For the case of the transition line closest to the ferromagnetic phase (see Fig. 18), the behavior of the fidelity susceptibility at criticality is quadratic implying that  $\nu = 1$ . Hence, in this region the model is in the same universality class as the transverse Ising model.

### V. SUMMARY AND CONCLUSIONS

We have studied the ground-state properties of the one-dimensional ANNNI model in a transverse magnetic field. The phase diagrams in the  $(J_2, B_x)$  plane were obtained using the quantum fidelity method for several lattice sizes. A picture emerged that is distinct from previously reported results. In addition to the known phases, namely, ferromagnetic, floating, and the  $\langle 2,2 \rangle$  phase, it seems that there will be an infinite number of modulated phases of spin sequences commensurate with the underlying lattice in the thermodynamic limit. We do not find paramagnetism for small values of the applied field. Paramagnetism is expected to occur at sufficiently high fields, not shown in our phase diagrams. The transitions between the modulated phases seem to be of second order. On the other hand, the transition between the floating and  $\langle 2,2 \rangle$  phase appears to be of first order.

### ACKNOWLEDGMENTS

We thank C. Warner for a critical reading of the manuscript. We also thank FAPERJ, CNPq, and PROPI (UFF) for

financial support. O.F.A.B. acknowledges support from the Murdoch College of Science Research Program and a grant

from the Research Corporation through Cottrell College Science Award No. CC5737.

- 
- [1] S. Sachdev, *Quantum Phase Transitions* (Cambridge University Press, Cambridge, 1999).
- [2] P. G. de Gennes, *Solid State Commun.* **1**, 132 (1963).
- [3] D. Bitko, T. F. Rosenbaum, and G. Aeppli, *Phys. Rev. Lett.* **77**, 940 (1996).
- [4] P. Pfeuty, *Ann. Phys. (N.Y.)* **57**, 79 (1970).
- [5] J. Simon, W. S. Bakr, R. Ma, M. E. Tai, P. M. Preiss, and M. Greiner, *Nature (London)* **472**, 307 (2011).
- [6] A. P. Young, *J. Phys. C* **8**, L309 (1975).
- [7] J. A. Hertz, *Phys. Rev. B* **14**, 1165 (1976).
- [8] M. Suzuki, *Prog. Theor. Phys.* **56**, 1454 (1976).
- [9] P. Rujan, *Phys. Rev. B* **24**, 6620 (1981).
- [10] M. N. Barber and P. M. Duxbury, *J. Phys. A* **14**, L251 (1981).
- [11] M. N. Barber and P. M. Duxbury, *J. Stat. Phys.* **29**, 427 (1982).
- [12] S. Suzuki, J. Inoue, and D. K. Chakrabarti, *Quantum Ising Phases and Transitions in Transverse Ising Models*, 2nd ed., Lecture Notes in Physics (Springer, Heidelberg, 2013).
- [13] A. Dutta, G. Aeppli, B. K. Chakrabarti, U. Divakaran, T. F. Rosenbaum, and D. Sen, in *Quantum Phase Transitions in Transverse Field Spin Models: From Statistical Physics to Quantum Information* (Cambridge University Press, Delhi, 2015).
- [14] C. M. Arizmendi, A. H. Rizzo, L. N. Epele, and C. A. Garcia, *Z. Phys. B* **83**, 273 (1991).
- [15] P. Sen, S. Chakraborty, S. Dasgupta, and B. K. Chakrabarti, *Z. Phys. B* **88**, 333 (1992).
- [16] H. Rieger and G. Uimin, *Z. Phys. B* **101**, 597 (1996).
- [17] P. Sen, *Phys. Rev. B* **55**, 11367 (1997).
- [18] P. R. Colares Guimarães, J. A. Plascak, F. C. Sá Barreto, and J. Florencio, *Phys. Rev. B* **66**, 064413 (2002).
- [19] A. Dutta and D. Sen, *Phys. Rev. B* **67**, 094435 (2003).
- [20] M. Beccaria, M. Campostrini, and A. Feo, *Phys. Rev. B* **73**, 052402 (2006).
- [21] M. Beccaria, M. Campostrini, and A. Feo, *Phys. Rev. B* **76**, 094410 (2007).
- [22] A. K. Chandra and S. Dasgupta, *Phys. Rev. E* **75**, 021105 (2007).
- [23] A. Nagy, *New J. Phys.* **13**, 023015 (2011).
- [24] M. E. Fisher and W. Selke, *Phys. Rev. Lett.* **44**, 1502 (1980).
- [25] S. Redner, *J. Stat. Phys.* **25**, 15 (1981).
- [26] W. Selke, *Phys. Rep.* **170**, 213 (1988).
- [27] I. Peschel and V. J. Emery, *Z. Phys. B* **43**, 241 (1981).
- [28] P. W. Anderson, *Phys. Rev. Lett.* **18**, 1049 (1967).
- [29] P. Zanardi and N. Paunković, *Phys. Rev. E* **74**, 031123 (2006).
- [30] C. H. Bennett, G. Brassard, and N. D. Mermin, *Phys. Rev. Lett.* **68**, 557 (1992).
- [31] D. F. Abasto, A. Hamma, and P. Zanardi, *Phys. Rev. A* **78**, 010301 (2008).
- [32] M. Cozzini, P. Giorda, and P. Zanardi, *Phys. Rev. B* **75**, 014439 (2007).
- [33] M. P. Nightingale, in *Finite-Size Scaling and Numerical Simulation of Statistical Systems*, edited by V. Privman (World Scientific, Singapore, 1990).
- [34] M. P. Nightingale, V. S. Viswanath, and G. Müller, *Phys. Rev. B* **48**, 7696 (1993).
- [35] O. F. de Alcantara Bonfim and J. Florencio, *Phys. Rev. B* **74**, 134413 (2006).
- [36] B. Boechat, J. Florencio, A. Saguia, and O. F. de Alcantara Bonfim, *Phys. Rev. E* **89**, 032143 (2014).
- [37] O. F. de Alcantara Bonfim, A. Saguia, B. Boechat, and J. Florencio, *Phys. Rev. E* **90**, 032101 (2014).
- [38] W. L. You and Y. L. Dong, *Phys. Rev. B* **84**, 174426 (2011).
- [39] D. Schwandt, F. Alet, and S. Capponi, *Phys. Rev. Lett.* **103**, 170501 (2009).
- [40] A. F. Albuquerque, F. Alet, C. Sire, and S. Capponi, *Phys. Rev. B* **81**, 064418 (2010).